Journal of Environmental Chemical Engineering 8 (2020) 104533

Contents lists available at ScienceDirect

Journal of Environmental Chemical Engineering

journal homepage: www.elsevier.com/locate/jece

Anti-quorum sensing and anti-biofilm activity of nickel oxide nanoparticles against *Pseudomonas aeruginosa*

Muthuchamy Maruthupandy [a], Govindan Nadar Rajivgandhi [b,*], Franck Quero [a], Wen-Jun Li [b,c]

[a] Laboratorio de Nanocelulosa y Biomateriales, Departamento de Ingeniería Química, Biotecnología y Materiales, Facultad de Ciencias Físicas y Matemáticas, Universidad de Chile, Avenida Beauchef 851, Santiago, Chile

[b] State Key Laboratory of Biocontrol, Guangdong Provincial Key Laboratory of Plant Resources and Southern Marine Science and Engineering Guangdong Laboratory (Zhuhai), School of Life Sciences, Sun Yat-Sen University, Guangzhou 510275, PR China

[c] State Key Laboratory of Desert and Oasis Ecology, Xinjiang Institute of Ecology and Geography, Chinese Academy of Sciences, Urumqi 830011, PR China

ARTICLE INFO

Editor: Despo Kassinos

Keywords:
Nickel oxide nanoparticles
Violaceum pigment degradation
Intracellular dysfunction
Scanning electron microscope
Toxicity assay

ABSTRACT

Nickel oxide nanoparticles (NiO NPs) were prepared by a chemical reduction method. The physical and morphological observations of NiO NPs were assessed by powder X-ray diffraction, thermogravimetric analysis, Fourier transform infrared spectroscopy, and UV–vis diffuse reflectance spectroscopy, scanning electron microscopy and transmission electron microscopy. Furthermore, the *in vitro* inhibition studies of violacein degradation in *Chromobacterium violaceum* ATCC 12472 and biofilm eradication in *P. aeruginosa* were detected at 50 μg/mL and 60 μg/mL, respectively. In addition, the biofilm inhibition was confirmed by ring biofilm degradation and time-kill variation assays. The live/dead cell variations, biofilm architecture damage and cell wall modifications of NiO NPs were investigated using confocal laser scanning microscope and SEM. In addition, NiO NPs were found to act as anti-biofilm agent against *P. aeruginosa*. Finally the *in-vivo* toxicity of NiO NPs was investigated against *Artemia franciscana*, suggesting low toxicity.

1. Introduction

Biofilms are complex enclosed microbial populations that adhere onto surfaces or interfaces. Biofilms have been identified as being involved in almost all human infections due to multi-drug-resistant (MDR) pathogens [1]. Biofilms are made up of many extracellular polymeric substances including complex polysaccharides, lipids and extracellular DNA [2]. The pathogenicity of biofilm producing bacteria is potentially effective against the human immune system. These bacteria can colonize the surface of medical implants and surgical instruments, as well as living tissues in lungs, wounds and bones due to the expression of polysaccharide matrices and phagocytosis-resistant genes of the cells [3]. The gene expression characteristic of bacteria within a biofilm are $\geq$ 1000 fold more resistant to antibiotics when compared to their planktonic counterparts [4]. Among important virulence factors, quorum sensing (QS) is involved in cell-to-cell communication that is produced during biofilm formation. ~300 genes are responsible for the QS regulation of *P. aeruginosa,* which is controlled by acylhomoserine lactones (AHL) [5]. QS may assist cell wall receptors during adherence and absorption activities [6]. Effective QS inhibitors can reduce the virulence of *P. aeruginosa* pathogenicity, and attenuate its pathogenesis, allowing the host immune system to manage infection. There is, however, an urgent need for new antimicrobial treatments as pathogenicity and virulence factors mediates immune responses.

Nowadays, numerous metal and metal oxide nanoparticles (NPs) can be synthesized. Metal oxide NPs have a widespread applications in various fields including sensor, electrochemical, food, anti-bacterial, anti-fungal and anti-cancer to cite a few only [7,8]. Metal oxide NPs possesses a wide range of potential applications owing to their attractive electrical, mechanical, optical, chemical properties [9]. Metal oxide NPs considerably differ in numerous features and properties from their bulk materials due to their size, shape, and high specific surface area as well as good electrical and magnetic properties [10]. Among metal oxide NPs, nickel oxide (NiO) NPs have been gaining more attention due to their multifunctional and tunable nature. NiO NPs are a p-type semiconductor, with a direct band gap value of 3.7–40 eV [11]. NiO NPs have been reported to possess excellent potential for use in biomedical application, more particularly for anti-biofilm application against various multi-drug resistant bacteria [12].

NiO NPs can be synthesized using different physical and chemical

* Corresponding author at: School of Life Sciences, Sun Yat-Sen University, Gunagzhou, China.
E-mail address: rajivgandhimicro@yahoo.com (G.N. Rajivgandhi).

https://doi.org/10.1016/j.jece.2020.104533
Received 22 August 2020; Received in revised form 16 September 2020; Accepted 21 September 2020
Available online 28 September 2020

methods; namely co-precipitation, chemical reduction, solvothermal, sol–gel and electro–deposition [13]. Among them, the chemical reduction method is unique since it is a simple and cost effective method for the synthesis of pure NiO NPs and these have been reported to possess high specific surface area at low temperature [14]. By choosing an appropriate precursor, surfactant and calcining method, NiO NPs with narrow size range and morphology can be obtained. Limited reports, however, are currently available for the synthesis of NiO NPs and their related toxicity and anti-biofilm activity. As a result, this study focuses on the synthesis and characterization of NiO NPs and their subsequent evaluation against biofilm forming *P. aeruginosa* through standard *in vitro* experiments and *in-vivo* toxicity.

2. Materials and methods

2.1. Synthesis of NiO NPs

Nickel chloride hexahydrate ($NiCl_2{\cdot}6H_2O$) (1.43 g) was dissolved in absolute ethanol and subsequently added to a flask containing 6.73 mL of 5 M hydrazine monohydrate solution. The pH of the mixture was adjusted between 8.0 and 12.0 using 1 N of potassium hydroxide. The mixture was continuously stirred for 2 h at 37 °C. The resulting product was subsequently washed using doubly distilled water to remove reaction residues, followed by washing with acetone. At the end of the process, dark green solid particles were obtained and dried in convection oven at 70 °C for 24 h. The nickel hydroxide solid particles were then converted to NiO NPs by thermal decomposition at 300 °C for 2 h [15].

2.2. Characterization of NiO NPs

UV–vis diffuse reflectance spectroscopy (DRS) absorption spectra of NiO NPs were monitored at 37 °C in the wavelength range of 200−800 nm using a UV–vis spectrophotometer (Shimadzu UV-2500, Japan) equipped with a diffuse reflectance accessory. The synthesized NiO NPs were characterized by Fourier transform infrared (FTIR) spectroscopy in the wavenumber range of 4000−400 cm^{-1} using a Nicolet FTIR (NEXUS-870, USA) spectrometer. Powder X-ray diffraction (XRD) patterns of NiO NPs were recorded in the diffraction angle 2θ range of 10−80° using a Rigaku D/max-RA X-ray diffractometer equipped with a Cu-Kα radiation (λ =1.54178 Å). Thermogravimetric (TGA) traces of NiO NPs were recorded using a TGA-7 Perkin-Elmer thermogravimetric analyzer under air atmospheric condition at a heating rate of 20 °C/min from 30 °C up to 800 °C. The composition and surface morphology of the samples were assessed using a scanning electron microscope (SEM, Hitachi S-4800, Japan) coupled with energy-dispersive X-ray spectroscopy (EDX). The structure, size and morphology of the synthesized materials were studied by transmission electron microscopy (Hitachi JEM-2100, Japan).

2.3. In-vitro inhibition studies

2.3.1. Antibacterial activity

The antibacterial effect of NiO NPs against biofilm producing *P. aeruginosa* was quantified by using agar well diffusion method [24]. Briefly, log phase cultures of biofilm producing *P. aeruginosa* were spread onto Mueller-Hinton agar (MHA) plates and wells were subsequently cut using gel puncture. Afterwards, different concentrations (5, 10, 15, 20, 25, 30, 35, 40, 45 and 50 µL) of NiO NPs were added separately into the wells. Distilled water and ceftazidime acted as negative and positive controls, respectively. After 24 h of incubation at 37 °C, the zones of inhibition around the wells were measured.

2.3.2. Violacein pigment degradation assay

The effect of NiO NPs on the violacein pigment degradation of *Chromobacterium violaceum* ATCC 12472 was studied by tube inoculation method [4]. Briefly, log phase cultures of *C. violaceum* ATCC 12472 were added to various concentrations (0, 10, 20, 30, 40, 50, 60, 70, 80, 90 and 100 µg/mL) of NiO NPs individually into 50 mL test tube. A *C. violaceum*-containing tube (without addition of NiO NPs) acted as control. All the tubes were incubated at 37 °C for 24 h. If the NiO NPs effectively stopped the violacein pigment degradation after 24 h exposure in the QS system, this means that the purple colored pigment was modified, which can be noticed visibly in the test tube. Decrease in the intensity of the purple color is indicated that the N-acyl-L-homoserine lactones (AHL) was degraded. No change in the intensity of the purple color wass indicative of non-QS inhibition in the QS system of the test tube.

2.3.3. Quantification of violacein inhibition

Similarly, the effect of the NiO NPs on the QS system was further confirmed by carrying out quantitative measurement of violacein inhibition using *C. violaceum* ATCC 12472 [5]. Briefly, a 24 h incubated *C. violaceum* ATCC 12472 culture was inoculated into a Luria-Bertani (LB) broth containing test tube and different concentrations (0, 10, 20, 30, 40, 50, 60, 70, 80, 90 and 100 µg/mL) of NiO NPs were added individually into test tubes. The different concentrations of NiO NPs treated or untreated non-violacein producing *C. violaceum* CV026 was used as a positive control. After 24 h, 1 mL of each culture tube was collected and centrifuged at 10,000 rpm for 15 min, allowing the violacein to precipitate. After precipitation, the pellet was collected and solubilized in 1 mL of dimethyl sulfoxide (DMSO) and vortexed vigorously to solubilize completely the violacein. The solubilized samples were centrifuged again to remove the cells and the extracted violacein pigment was subsequently quantified using UV–vis spectrophotometer by measuring the optical density (OD) of control and test samples at a wavelength of 570 nm. The percentage of violacein inhibition was estimated using the formula

$$\text{Percentage of inhibition} = [(\text{Control OD 570 nm} - \text{Test OD 570 nm})/\text{Control OD 570 nm}] \times 100 \quad (1)$$

2.3.4. Attenuation of violacein inhibition

The QS inhibition ability of NiO NPs was further validated through enzyme treatment or heat loss attenuation method as reported before by Rajivgandhi et al. [16]. 100 µL of NiO NPs was treated with proteinase K at 95 °C in a hot air oven to suppress their inhibition ability. Tubes without attenuated NiO NPs treated *C. violaceum* ATCC 12472 acted as positive control. After 5 h, all the attenuated and non-attenuated NiO NPs were inoculated into the *C. violaceum* ATCC 12472 containing test tube. All the tubes were subsequently incubated at 37 °C for 6, 12 and 24 h. After incubation, all the test tubes were analyzed for detection of violacein in *C. violaceum* ATCC 12472. The non-attenuated NiO NPs treated *C. violaceum* ATCC 12472 showed a change in the intensity of the purple color that originate from the pigment. Attenuated NiO NPs treated *C. violaceum* ATCC 12472 exhibited an unchanged intensity of the purple color, which indicated that the NiO NPs had anti-QS activity due to the AHL degradation. The percentages of the attenuated and non-attenuated NiO NPs treated *C. violaceum* ATCC 12472 were calculated to quantify the anti-QS activity of NiO NPs. OD values of control and test samples were determined by UV–vis spectrophotometry and the percentages were calculated using formula (1).

2.3.5. Biofilm inhibition assay

The disruption of biofilm using NiO NPs against *P. aeruginosa* was studied by 24 well polystyrene plate method [2]. Briefly, *P. aeruginosa* culture in addition of various concentrations (10−150 µg/mL) of NiO NPs were taken together in tryptic soy broth (TSB) at 37 °C for 24 h. The wells without addition of the NiO NPs acted as control. After washing with PBS, the sample was stained with 500 µL of 0.4 % crystal violet

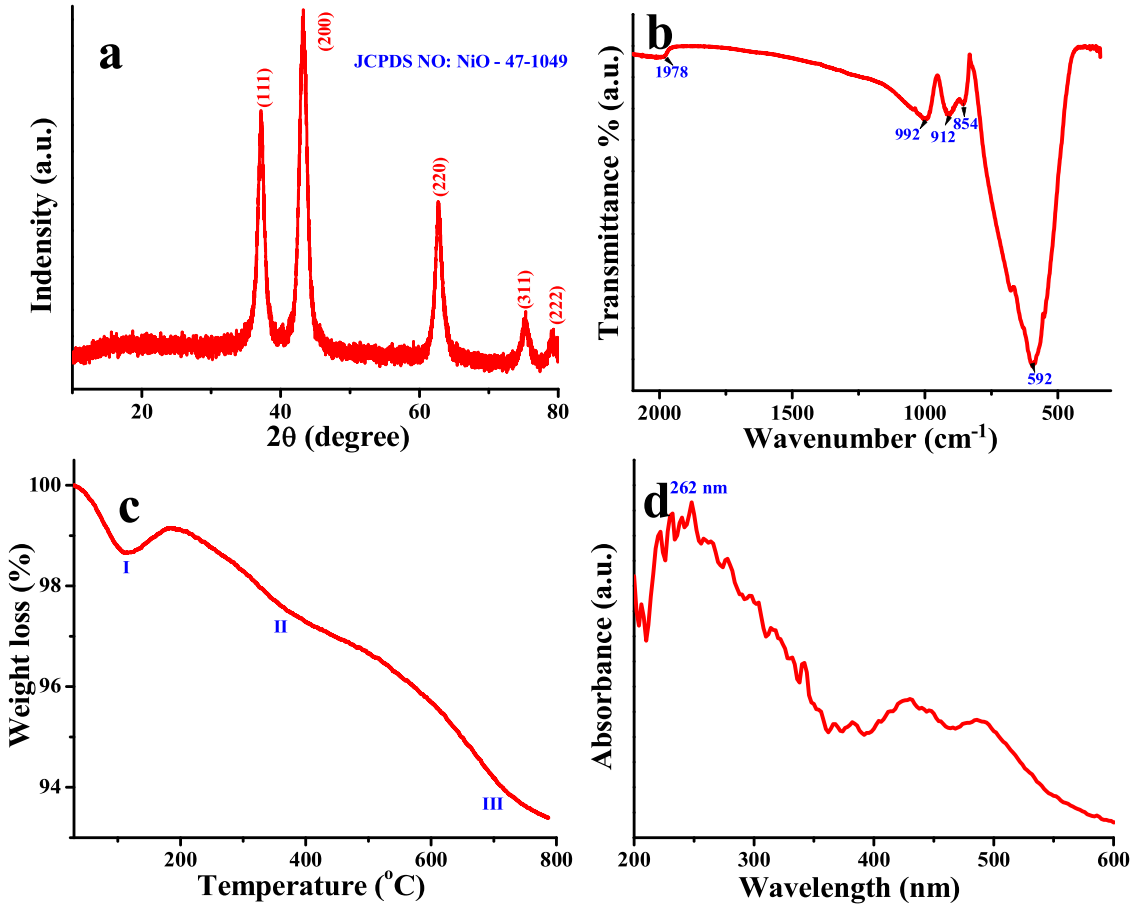

Fig. 1. Powder X-ray diffraction pattern (a), Fourier transform infrared spectrum (b), thermogravimetric analysis trace (c) and UV–vis diffuse reflectance spectrum (d) for NiO NPs.

(CV) solution for 30 min. The wells were subsequently rinsed twice with deionized water and allowed to air-dry. Finally, 1 mL of absolute ethanol was added into each well and the OD value was measured by UV–vis spectrophotometry at 570 nm. The experiment was performed in triplicate. The percentage of biofilm inhibition, equivalent to the biofilm inhibition concentration (BIC), was estimated using formula (1).

2.3.6. *Ring biofilm inhibition assay*

The disruption of biofilm formation was qualitatively analyzed by using ring biofilm assay based on the modified method of Kannappan et al. [3]. Briefly, 10 mL of stalled culture was added into the freshly prepared TSB tube supplemented with 1% of sucrose. BIC of NiO NPs was also added to the same well at 37 °C for 24 h. Tubes without addition of NiO NPs acted as control. After incubation, the tubes were stained with 0.4 % crystal violet solution and observed for the formation of a ring in the control tube as well as the potential degradation of the ring in treated tube.

2.3.7. *Time variation killing assay*

The different time intervals of NiO NPs against *P. aeruginosa* were determined by time-kill assay [26]. The log phase culture of *P. aeruginosa* was grown in LB broth and incubated at 37 °C for 24 h. After incubation, the cells were centrifuged and Rosewell Park Memorial Institute (RPMI) 1640 medium (1×10^6 cells/mL) was subsequently added. Then, the cells were incubated with various concentrations of NiO NPs at 200 rpm. The appropriate number of samples was collected from the incubated culture at respective time intervals of 0, 3, 6, 12, 18 and 24 h. All the collected samples were serially diluted, and the cell suspensions were platted on MHA at 37 °C for 24 h. After incubation, the growing colonies of the MHA plates were counted and calculated.

2.3.8. *Live/dead cell images*

1 mL of *P. aeruginosa* culture was transferred to a 6-well plate with a sterile cover slip (13 mm) along with BIC of NiO NPs. and culture without the addition of NiO NPs, acting as control, were maintained at 37 °C for 24 h. After incubation, the cover slips were taken out and washed twice with 3 mL of 0.9 % saline solution. Both cover slips were subsequently stained with 1.5 mL of 0.8 μM SYTO9 green fluorescent dye and 10 μM propidium iodide (PI) red fluorescent dye of live/dead staining kit (Live/dead ® BacLight™Bacterial Viability, ThermoFischer Scientific), and viewed by confocal laser scanning microcopy (CLSM, LSM 710, Carl Zeiss, Jena, Germany) for detection of live/dead cells using excitation/emission OD in the wavelength range of 480−600 nm [27].

2.3.9. *Confocal laser scanning microscope (CLSM)*

Log phase cultures of *P. aeruginosa* were inoculated into fresh sterilized TSB with or without addition of BIC of NiO NPs at 37 °C for 24 h. The untreated bacterial culture with TSB acted as control. After incubation, the cells were separated by centrifugation at 5000 rpm for 30 min and the separated cells were washed twice in PBS solution. After washing, the cells were stained with a 20 μL of mixed acridine orange/ethidium bromide dye in 10 mL of PBS at pH = 7.4 for 15 min under dark condition. The cells were rinsed with fresh PBS and stained cells were subsequently transferred onto a glass slide and subsequently viewed by using CLSM (Carl Zeiss, Jena, Germany) equipped with an argon laser having a wavelength of 488 nm, a 500–640 nm band pass emission filter and a ×100 objective lens [28].

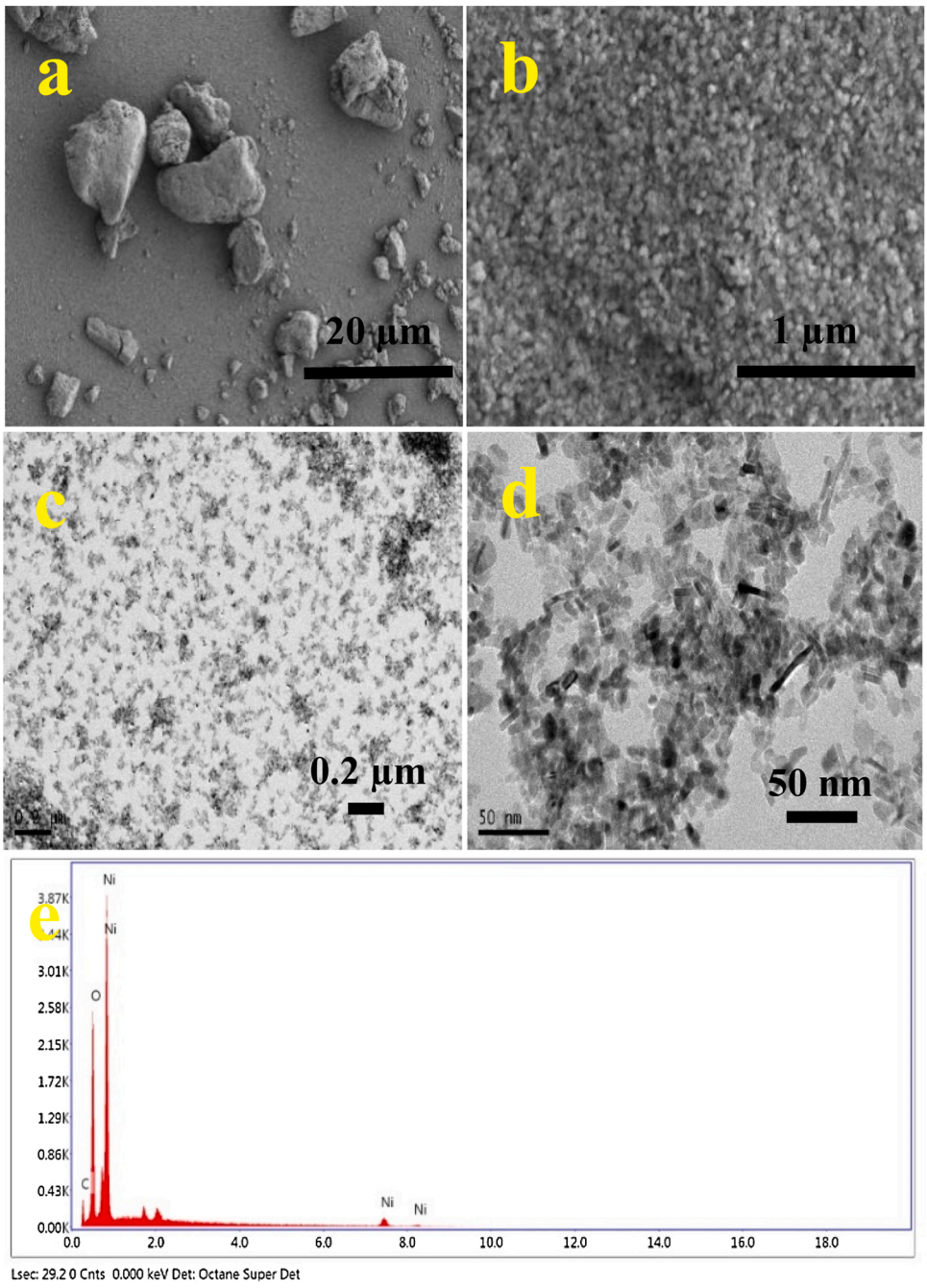

Fig. 2. High and low magnification scanning electron microscopy (a, b) and transmission electron microscopy (c, d) micrographs for NiO NPs, respectively. Energy dispersive X-ray spectrum (e) of NiO NPs.

2.3.10. Scanning electron microscope (SEM)

The morphological variation of *P. aeruginosa* at BIC of NiO NPs treated slide was observed by using SEM [29]. The cover slip of biofilm inhibition assay was subsequently washed with 10 mM sodium phosphate buffer (pH 7.4). The cells were then fixed with an equal volume of 4% glutaraldehyde for 4 h at 37 °C followed by washing twice in the PBS solution. The fixed cells were vacuum filtered using 0.1 mm thick polycarbonate membrane filters and dehydrated in ethanol-graded series (10, 20, 30, 40, 50, 60, 70, 80, 90 and 100 %). The cover slip was then dried and mounted onto an aluminium specimen support and coated with 15 nm thickness of gold-palladium metal (60:40 alloy). Finally, the sample was observed at an accelerating voltage of 20 kV (VEGA3 TESCAN, Brno, Czech Republic).

2.3.11. In-vivo toxicity analysis

The *in-vivo* toxicity of synthesized NiO NPs was assessed against *Artemia franciscana* (*A. franciscana*) following the method of Mishra et al. [30]. Briefly, the nauplii were hatched in 1 L glass tank and stocked at a concentration of 1 g/L cystein in filtered and sterilized marine water with 35 % salinity, pH = 8–8.2 and essential aeration for 24 h. After incubation for hatching, the aeration was stopped and the nauplii were caught using light emission and subsequently used for toxicity identification. Various concentrations of 10, 20, 30, 40, 50, 60, 70, 80, 90 and 100 µg/mL of NiO NPs were prepared from 1 mg/mL stock solution and exposed to 50 mL of sterile marine water containing a number of ten *A. franciscana* in a beaker with proper growth conditions (pH, salinity, temperature, *etc.*). Sample toxicity was determined based on the rate of nauplii death, which was classified by the absence of swimming activity

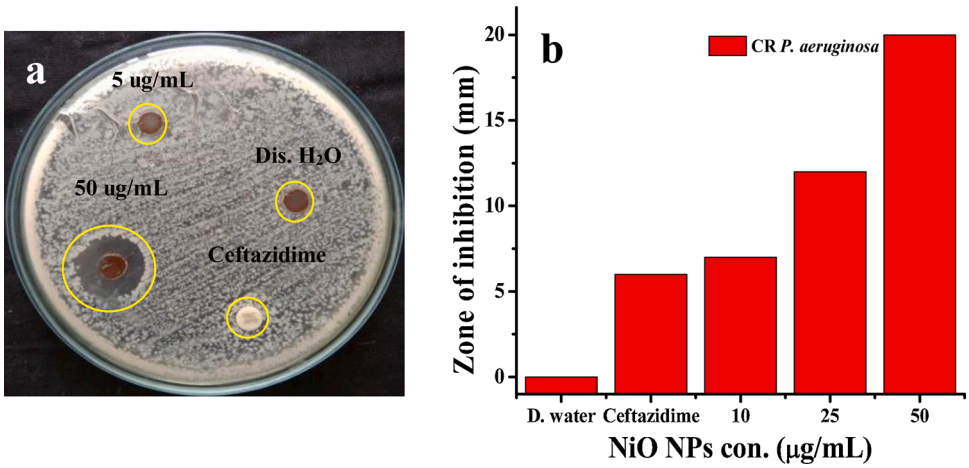

Fig. 3. Zones of inhibition for NiO NPs at various concentrations by agar well diffusion method (a) and the measurement of zone values obtained at 10, 25 and 50 μg/mL NiO NPs concentration (b).

in the experimental samples. The results were interpreted based on the rules and regulations of the Food and Drug Administration (FDA) and the following toxicity scale was used; 10 μg/mL concentrations were classified as nontoxic; 50 μg/mL were classified as moderately toxic and above 60 μg/mL concentration were considered as toxic. In addition, morphological alteration of *A. franciscana* lungs upon NiO NPs treatment was observed by using inverted light microscopy (Micros, Austria). The percentage of mortality and the median lethal dose (LD_{50}) for the tested concentration of NiO NPs was determined using a probit analysis and survival rate.

3. Results and discussion

3.1. Characterization of NiO NPs

The phase composition, purity and crystalline structure of the synthesized NiO NPs were assessed by powder XRD analysis (Fig. 1a). A typical powder XRD pattern for NiO NPs is reported in Fig. 1a and displays diffraction peaks located at diffraction angle 2θ positions of ~37.1°, 43.3°, 62.8°, 75.2° and 79.2°, corresponding to (111), (200), (220), (311), and (222) diffraction planes, respectively. The powder XRD diffraction peaks suggested a high crystallinity with a face-centered cubic arrangement of NiO. All the diffraction peaks were found to match with JCBDS Card file No: 47-1049 [14]. Fig. 1a suggests that relatively small NiO particles were synthesized due to the relatively wide width of the diffraction peaks. Additionally, no additional peaks were detected that could potentially correspond to impurities that possess crystalline or semi-crystalline structure, including $Ni(OH)_2$. As a result, unreduced $Ni(OH)_2$ was not identified after carrying out the synthesis process, which suggests that highly pure NiO NPs were successfully formed.

FTIR spectroscopy is a relevant characterization technique for demonstrating the potential presence of potential functional groups at the surface of the synthesized NiO NPs. Fig. 1b displays a typical FTIR spectrum for NiO NPs. Absorption bands can be observed at wavenumber positions of ~1978, 992, 912, 854 and 592 cm^{-1}. The FTIR bands located at wavenumber positions of ~1978 and 992 cm^{-1} were found to correspond to the vibrational motions of C═C═C and CO—O—CO moieties, respectively. The absorption bands located at ~912 and 854 cm^{-1} were found to correspond to C═C and O—C═O symmetric and asymmetric stretching vibrations, respectively. The absorption band located at a wavenumber position of ~592 cm^{-1} corresponds to the vibrational motions of Ni—O bonds, suggesting the successful formation of NiO NPs that possess organic functional groups at their surface.

TGA was used to examine the thermal stability of the synthesized NiO NPs. The TGA curve of NiO NPs is shown in Fig. 1c. Three weight losses were found to occur at temperatures of ~107 °C (I), 385 °C (II) and 680 °C (III). The first weight loss that occurred at ~107 °C can be attributed to the evaporation of water molecules. The second weight loss that occurred at ~385 °C may be attributed to the following degradation reaction ($Ni(OH)_2 \rightarrow NiO + H_2O$) [22]. The third weight loss was observed at ~680 °C, which may be associated to the loss of more tightly bounded water molecules. The thermal weight loss percentage of the NiO NPs was found to be ~0.86 %, ~2.44 %, and ~3.16 % at temperatures of ~109 °C, 385 °C, and 680 °C, respectively. The total percentage weight loss of NiO NPs was 6.61 %. Therefore, the synthesized NiO NPs possess, as expected, high thermal stability.

The optical properties of the synthesized NiO NPs were examined by UV–vis diffuse reflectance spectroscopy (UV-DRS) and a typical spectrum is reported (Fig. 1d.). An absorption peak can be observed at a wavelength of ~262 nm, which represents the photoreaction of the NiO NPs in the UV light range. Similar absorption peak positioned in the UV range have been reported previously for NiO NPs [23].

The morphology of NiO NPs was imaged using SEM, and the resulting images are shown in Fig. 2a, b. From these images, the morphology of NiO NPs is hard to define and unclear. One can observe, however, some agglomerated structures (Fig. 2a) that are actually formed by small particles (Fig. 2b). This might be due to the synthesis process and the consequences of calcification temperatures. The response time and temperature are two vital factors influencing the shape of the NPs. The same accumulation of the NPs was not found for NiO NPs submitted to a temperature of 300 °C for 2 h.

Due to the poor information provided by SEM analysis, the structural morphology and size of the synthesized NiO NPs was observed by TEM analysis (Fig. 2c, d). The TEM images of NiO NPs show a rod-like morphology with a width size of ~3 nm. The monodispersed size of the NiO NPs (Fig. 2d) could be visibly identified, which might be due to the thermal calcinations of Ni at 300 °C, which is adequate for accumulation due to the high surface energy of the NPs. The elemental configuration of NiO NPs was determined using EDX spectroscopy. The characteristic EDX spectrum for NiO NPs is shown in Fig. 2e. The EDX spectrum of NiO NPs allowed the qualitative and quantitative analysis of the composition of NiO NPs. NiO NPs had atomic percentages of 53.25 % for Ni and 46.75 % for O, and atomic weights of 77.11 % for Ni and 20.84 % for O (Fig. 2e). The synthesized NiO NPs did not include any elements other than Ni and O. As a result, relatively pure NiO NPs were successfully synthesized using this simple method.

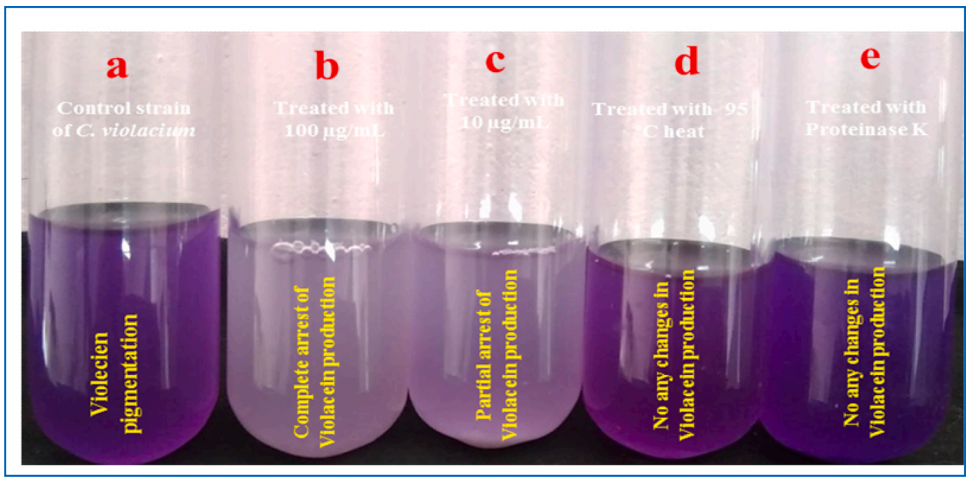

Fig. 4. QS inhibition effect of NiO NPs against *C. violaceum* 12472 control (a), and treated with 50 µg/mL (b) and 10 µg/mL (c), and heated at 95 °C (d) and treated with proteinase K (e).

3.2. *In-vitro inhibition study*

3.2.1. *Antibacterial activity*

After 24 h incubation, the wells of MHA plates exhibited 20 mm zone of inhibition at a concentration of 50 µg/mL. The control well containing distilled water did not show any zone of inhibition and the positive control of ceftazidime showed a 6 mm zone of inhibition. Interestingly, 7 and 12 mm zone of inhibition were observed at 10 and 25 µg/mL concentrations of NiO NPs, respectively. This result implies that the antibacterial effect of NiO NPs started being efficient at relatively low concentrations (Fig. 3 a, b). When the cells were exposed to higher concentrations, all the three lag, log or exponential and stationary phases were restricted in terms of the growth of bacterial colonies. Therefore, the result clearly suggests that the NiO NPs possess antibacterial property against biofilm forming *P. aeruginosa* at increasing concentrations. Recently, Suresh et al. reported that NiO NPs have similar growth inhibition effect against MRSA, *P. aeruginosa,* and *E. coli* [24]. Recently, NiO NPs were found to exhibit 11 and 12 mm inhibition zones against *E. coli* and *K. pneumoniae*, respectively, at 50 µg/mL concentration [14]. Helan et al. [15] reported that the more lipopolysaccharide produced *E. coli* and *S. aureus* was inhibited by NiO NPs, and the bacteria *E.coli* exhibited 11 mm zone of inhibition. In addition, the NiO NPs inhibit the bacteria in a concentration dependent manner, and possess the potential ability to permeate into the cell wall of bacteria. NiO NPs were found to damage the cytoplasmic layers and other inner cellular components, causing cell death.

The action mechanism of NiO NPs against gram-negative bacteria (GNB) was recently reported by Khawlah et al. [25]. When the NiO NPs attach to the surface of GNB, the permeability and intracellular damage was enhanced, modifying the transport mechanism through cytoplasmic leakages in the inside of the cells. It was assumed that the GNB cell wall could be easily degraded by the small size of the NiO NPs, leading them inside the cells and causing cell death due to the enzyme deactivation and H_2O_2 production [26]. Our result agrees with those of Yung et al. [27], suggesting that after the entry of nanoparticles into the cell wall, the sulphur and phosphorous compounds including proteins and DNA collapsed. The anti-bacterial efficiency originated from the NiO NPs by binding to the GNB surface, stimulating the respiration process and leading to enzyme degradation [28]. Therefore, the result suggests that the NiO NPs possess excellent antibacterial activity against biofilm forming *P. aeruginosa*.

3.2.2. *Violacein pigment degradation assay*

The inhibition of violet pigmentation *C. violaceum* ATCC 12472 treated with NiO NPs confirmed that the NiO NPs have QS inhibition ability. The result reported in Fig. 4, indicates that 50 µg/mL of NiO NPs clearly stops the violacein production in *C. violaceum* ATCC 12472 without affecting the bacterial growth when compared to the control. After 24 h incubation, the complete and partial degradation of violacein pigment was observed at 50 µg/mL and 10 µg/mL treated tubes (Fig. 4d, e). In contrast, no pigment degradation was observed for the control tube (Fig. 4c). These results are more evident than those previously reported [29,30], including some others, which reported that NiO NPs did not improve QS inhibition at 50 µg/mL, with violacein inhibition equal to 0%. Therefore, the present result indicated that the NiO NPs can disrupt QS components including AHL-dependent QS communication systems. The results of this study confirmed the potential advantages of the NiO NPs, due to their low turbidity, high solubility and high stability over other conventional NPs [5,31].

3.2.3. *Quantification of violacein inhibition*

The degradation of violacein in the NiO NPs treated *C. violaceum* ATCC 12472 was monitored quantitatively by UV–vis spectrophotometry. After centrifugation as well as 12 and 24 h incubation, the extracted violacein pigment was found to be 92 % at 50 µg/mL. However, the addition of NiO NPs with C6-HSL to *C. violaceum* CV026 resulted in 90 % violacein inhibition at 60 µg/mL. The test samples were analyzed to quantify the potential disruption of the AHL-dependent QS communication systems and calculate the amount of inhibition in the violacein pigment production based on the purple color variation (Fig. 4a, b). The differences between *C. violaceum* ATCC 12472 and the positive control of C6-HSL supplemented *C. violaceum* CV026 were significant when compared with control *C. violaceum* CV026 (without addition of C6-HSL). This also suggested that both the strains significantly lost the violacein pigment upon increasing concentration. Similar result was obtained by Akyuz et al. [32], where a significant reduction in violacein pigment accompanied by turbid purple color in NiO NPs treated *C. violaceum* ATCC 12472 was detected for NiO NPs at 100 µg/mL. In addition, our result suggests that the NiO NPs have inhibition ability in violacein production of up to 90 %, which indicates that NiO NPs possess a strong and long-term QS inhibition ability at a relatively low concentration of 50 µg/mL. This is lower than previously reported NiO NP results [33,34]. Previously, Rajivgandhi et al. [16] reported that the QS effectively regulated the violacein pigmentation and biofilm formation due to the AHL communication system. Therefore, the results indicate the potential of synthesized NiO NPs as novel QS-based antibacterial material and suitable alternative over conventional antibacterial agents.

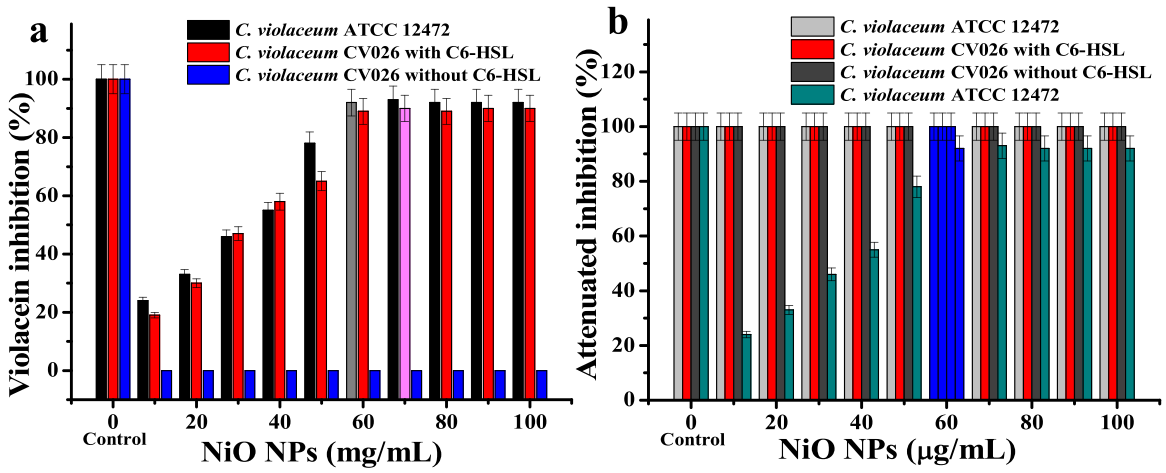

Fig. 5. QS inhibition effect of NiO NPs (a). No changes of the attenuated NiO NPs against *C. violaceum* CV026 were observed (b).

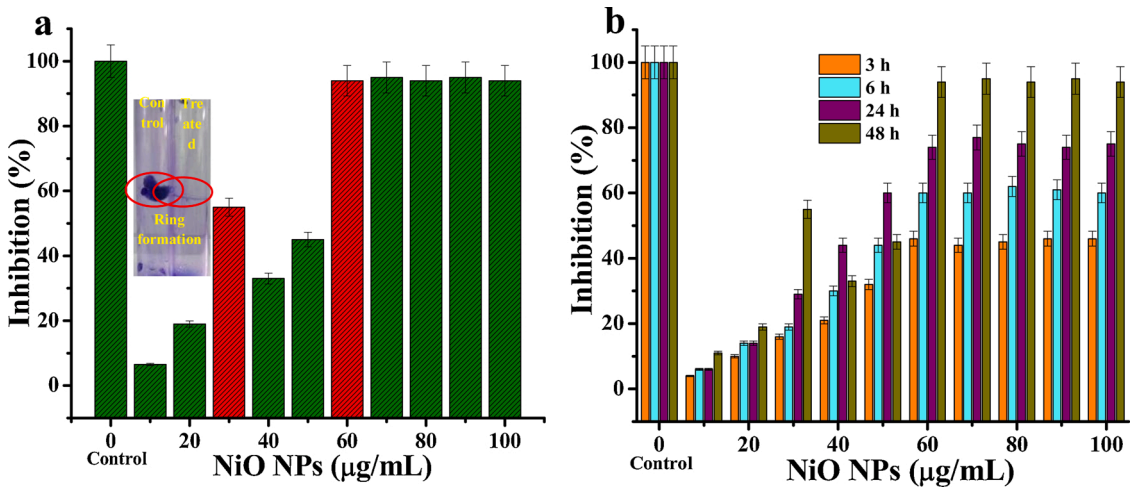

Fig. 6. Anti-biofilm activity of NiO NPs against *P. aeruginosa* at various concentrations (a) and the time-dependent variation of anti-biofilm activity (b).

3.2.4. Attenuation of violacein inhibition

The anti-QS effect of NiO NPs was further validated by following the attenuation process of violacein inhibition and the results are shown in Fig. 5. After 5 h exposure to proteinase K and NiO NPs previously exposed to a temperature of 95 °C, *C. violaceum* ATCC 12472 did not show any changes in cell density when compared with that of positive control (Fig. 5a, b). At all the tested concentrations, the attenuated NiO NPs lost their QS inhibition ability against *C. violaceum* ATCC 12472 and exhibited similar OD values as the control. This is possibly due to the continuous communication and persistence of pathogenicity in the tested broth culture. This result made clear that the NiO NPs did not have a bactericidal effect against *C. violaceum* ATCC 12472. Furthermore, the loss of native QS inhibition effects in the presence of proteinase K and heat treated NiO NPs was observed with no depolarization and inhibition or cell biomass in the QS positive isolates. However, both the attenuated experimental results confirmed that the tested samples lost their QS inhibition level and experienced QS activity. This provides further evidence that the unmodified NiO NPs have QS inhibition ability (Fig. 5g). In addition, the absence of QS inhibition and inactivation of AHLs production upon applying heat treatment provides evidence of possible enzymatic activity for NiO NPs. This result is roughly agrees with previous reports by Rajkumari et al. [35] and Alipour et al. [36], who modified complex molecules of NiO NPs against *C. violaceum* ATCC 12472 resulting in higher QS inhibition at 70 µg/mL and 100 µg/mL. Therefore, it was found that the NiO NPs possess anti-QS activity against MDR bacteria due to possible enzymatic inhibition activity [37]. In addition, NiO NPs may participate in AHL modification as well as biofilm inhibition process.

3.2.5. Inhibition of biofilm formation

The concentration dependent biofilm inhibition abilities of NiO NPs was observed against strong biofilm producing *P. aeruginosa* (Fig. 6a). After 24 h treatment, 94 % of biofilm inhibition against *P. aeruginosa* at 60 µg/mL of NiO NPs was observed compared to the control. This result indicates that the NiO NPs possess inhibition ability upon increasing NiO NPs' concentration. Therefore, 60 µg/mL of NiO NPs was fixed as the biofilm inhibition concentration (BIC) for the *P. aeruginosa* strain. Recently, in our previous report of NiO NPs and ZnO nanosheet, it was found that biofilm formation was inhibited at 100 µg/mL concentration against ciproflaxacin resistant *E. coli* and *P. mirabilis* [38]. This result suggested that the colonization and cell bundles of biofilm architecture in *P. aeruginosa* totally collapsed due to NiO NPs treatment. Argueta-Figueroaa et al. [39] reported that the maximum biofilm disruption against strong biofilm forming MRSA was 77 % at 500 µg/mL. As reported by Soumyadipta et al. [40] NiO NPs inhibited the ESBL produced biofilm, forming uropathogens at highest concentration. Finally, our result suggests that the NiO NPs enhances the biofilm inhibition without affecting the growth of the bacteria, which may alter the various signaling mechanisms in biofilm formation.

Table 1
Comparative investigations of anti-biofilm activity of NiO NPs against various bacterial strains reported in previous studies.

Sample	Test Organisms	ZOI (mm)	Concentration (μg/mL)	MIC (μg/mL)	MBC (μg/mL)	Time Interval (h)	References
NiO NPs	*P. aeruginosa* and *B. subtilis*	18 and 21	8	8	16	24	[40]
n-NiO NPs	*S. aureus* and *P. aeruginosa*	6 and 18	100	60 and 80	60 and 80	24	[24]
Nickel Hydroxide nanoparticles NPs	*E.coli*	5	80	80	80	24	[28]
NiO NPs	*E. coli* and *K. pneumoniae*	15	50	50	50	24	[14]
NiO NPs	*B. subtilis, S. aureus* and *E. coli*	10, 10 and 19	90	120	120	24	[39]
NiO NPs	*P. aeruginosa* and *B. subtilis*	18	50	8 and 32	8 and 32	24	[41]
NiO NPs	*E. coli, K. pneumonia* and *P. typhus*	4, 7 and 4	100	100	100	24	[28]
NiO NPs	*S. aureus* and *E. faecalis*	10	10	10	10	24	[40]
NiO NPs	CR *P. aeruginosa*	20	50	60	60	24	**Present Study**

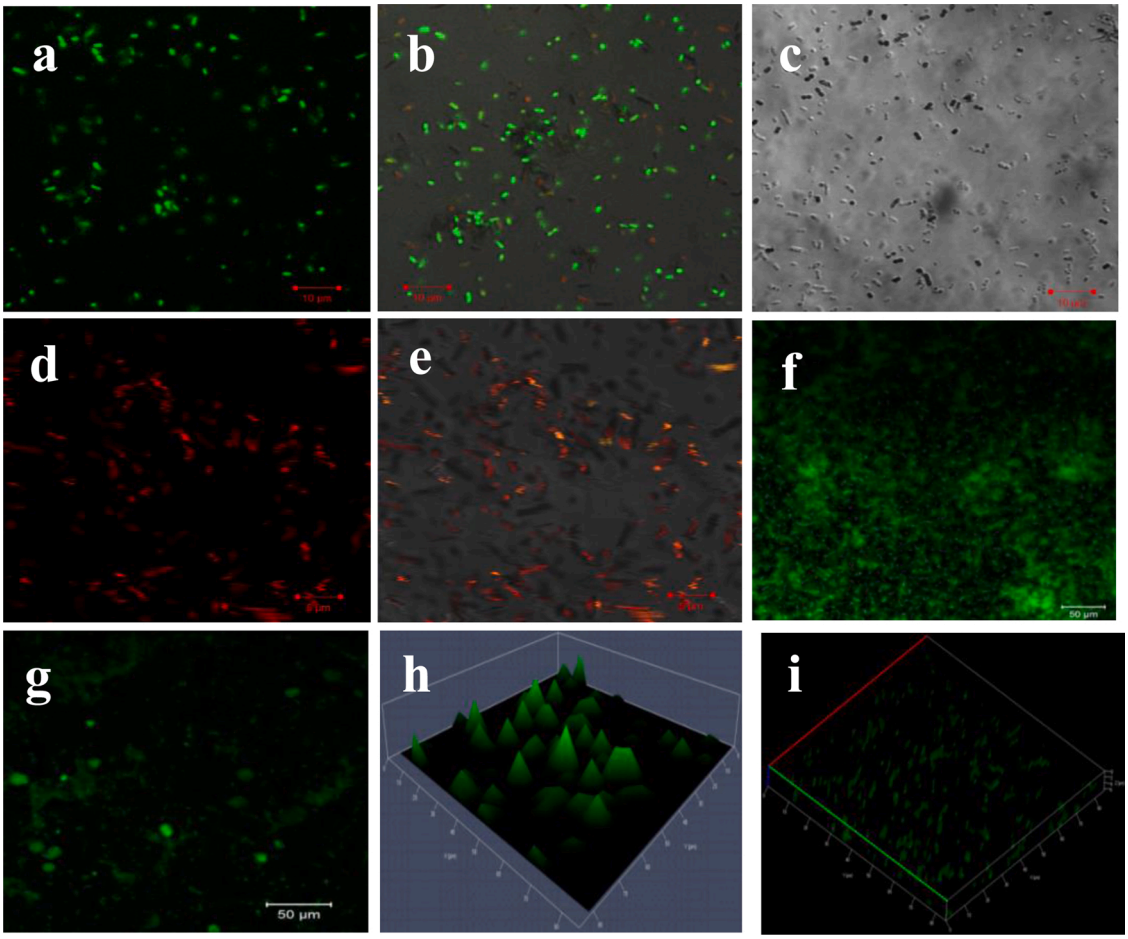

Fig. 7. Live/dead cell variation at biofilm inhibitory concentration for NiO NPs treated with CR *P. aeruginosa* in the control exhibited a green color (a). The cell density identification (b), phase contrast variation (c), treated image from confocal laser scanning microscopy (d), and phase contrast (d) were observed. The anti-biofilm effect of the untreated control *P. aeruginosa* as 2D and 3D images (e, f) and treated with NiO NPs as 2D and 3D images (g, h) as observed by confocal laser scanning microscopy.

3.2.6. Ring biofilm inhibition assay

After 24 h incubation, the rigidity of the *P. aeruginosa* biofilm degraded in the NiO NPs treated tube when compared to the control. Furthermore, the visualization of ring formation in the treated or untreated test tubes confirmed that the NiO NPs have anti-biofilm effect (Insert Fig. 6). The ring biofilm inhibition assay mostly correlated with TCP assay, and evidenced that the BIC level of NiO NPs as an effective concentration against *P. aeruginosa*. A similar result was reported by Kannappan et al. [3], where biofilm ring formation was degraded at increasing dose.

3.2.7. Time kill variation assay

The anti-biofilm effect of NiO NPs was further validated, and the result of time-kill assay revealed that the NiO NPs have excellent inhibition effects at various time intervals. At the BIC, the NiO NPs exerted remarkably rapid killing effects against *P. aeruginosa* after 3 h and eventually killed the cells at the limit of detection. After 6 h incubation, the bacterial culture reached log phase, followed by the decline phase

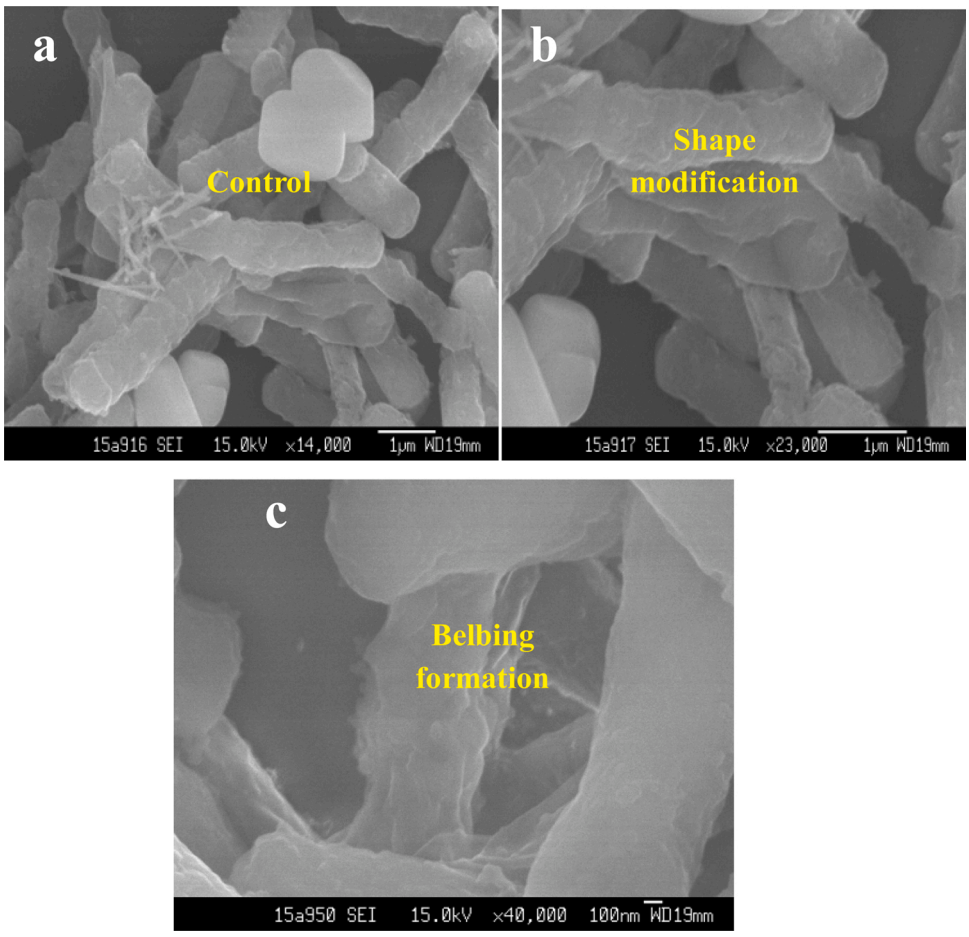

Fig. 8. Morphological damage of the biofilm-forming untreated *P. aeruginosa* (a), and NiO NP-treated *P. aeruginosa* (b, c) as observed by scanning electron microscopy..

and finally reached the death phase at 12 h. After 24 h, the entire biofilm formation was eradicated at the BIC of NiO NPs. This result showed a rapid rate of killing and excellent efficacy of NiO NPs against *P. aeruginosa* upon increasing concentrations (Fig. 6b). The enhanced killing rate and efficacy might be influenced by interaction of the NiO NPs compared to the control. The cell suppression in the exponential phase of the CR *P. aeruginosa* suggests a bacteriostatic effect of NiO NPs. Recent studies of concentration- and time-dependent biofilm inhibition are presented in Table 1.

3.2.8. *Live/dead cells images*

The live and dead cell variations of NiO NPs treated or untreated *P. aeruginosa* are depicted in Fig. 7. The results clearly reveal that the treated cover slip images show low adherence at desired BIC (Fig. 7a, b). Similar cell densities were also reduced as compared with untreated control cells (Fig. 7a–c), indicating the inhibitory effect of NiO NPs treated *P. aeruginosa* cells associated with a greater number of bacterial death. The number of cell death was significantly higher for BIC treated cells when compared to the untreated control cells. In addition, the changes in the confluent layer with loosely packed death cells on the cover slips were detected in treated cells [41]. In the mechanistic approach, the SYTO9 stain was used to bind into the total nucleic acid content inside the cells. The dead cells were identified by pink color, and live cells were identified with a green color. Propidium iodide (PI) dye was unable to penetrate the cytoplasmic membranes of healthy cells and produced a red color in dead cells [42]. In our study, the inhibition effect at 60 μg/mL is a two-fold improvement compared to previous reports [14,43].

3.2.9. *Confocal laser scanning microscope*

The damaged architecture and surface topography of NiO NPs (BIC) treated *P. aeruginosa* was clearly observed using CLSM. The images are presented in Fig. 7. After treatment with 60 μg/mL of BIC, the test and control samples were stained with AO for live and dead cells identification. Highly dispersed, drastically disturbed colonies were observed in the treated cell sample (Fig. 7d). In contrast, the smooth membrane morphology, depicting well-integrated structures were observed in the control strain sample (Fig. 7e). At BIC, NiO NPs were strongly attached onto the surface of the *P. aeruginosa* compared to the control and a green color was observed in the CLSM images. Therefore, the results confirmed that the NiO NPs strongly enhanced the anti-biofilm effect against *P. aeruginosa*. The 3D image (Fig. 7f) of the treated cells confirmed that the strong attachment of NiO NPs onto the *P. aeruginosa* surface totally mismatched the biofilm architecture arrangement due to the lower rate of cellular aggregation. The loss of cellular adherence during the treatment of NiO NPs was considered as a significant factor for higher rate of biofilm disintegration when compared to the control (Fig. 7h). A recent study by Maruthupandy et al. [18] found that AO stain is an excellent dye for the detection of intense biofilm-forming cells in CLSM. The strong attachment of NiO NPs onto the biofilm-forming bacterial surface was used to identify the damaged biofilm morphology in 3D using CLSM [44].

3.2.10. *Scanning electron microscope*

The control and test SEM images are reported in Fig. 8. After dehydration, an irregular surface, membrane collapse, the formation of rumples and the loss of membrane integrity were observed in treated

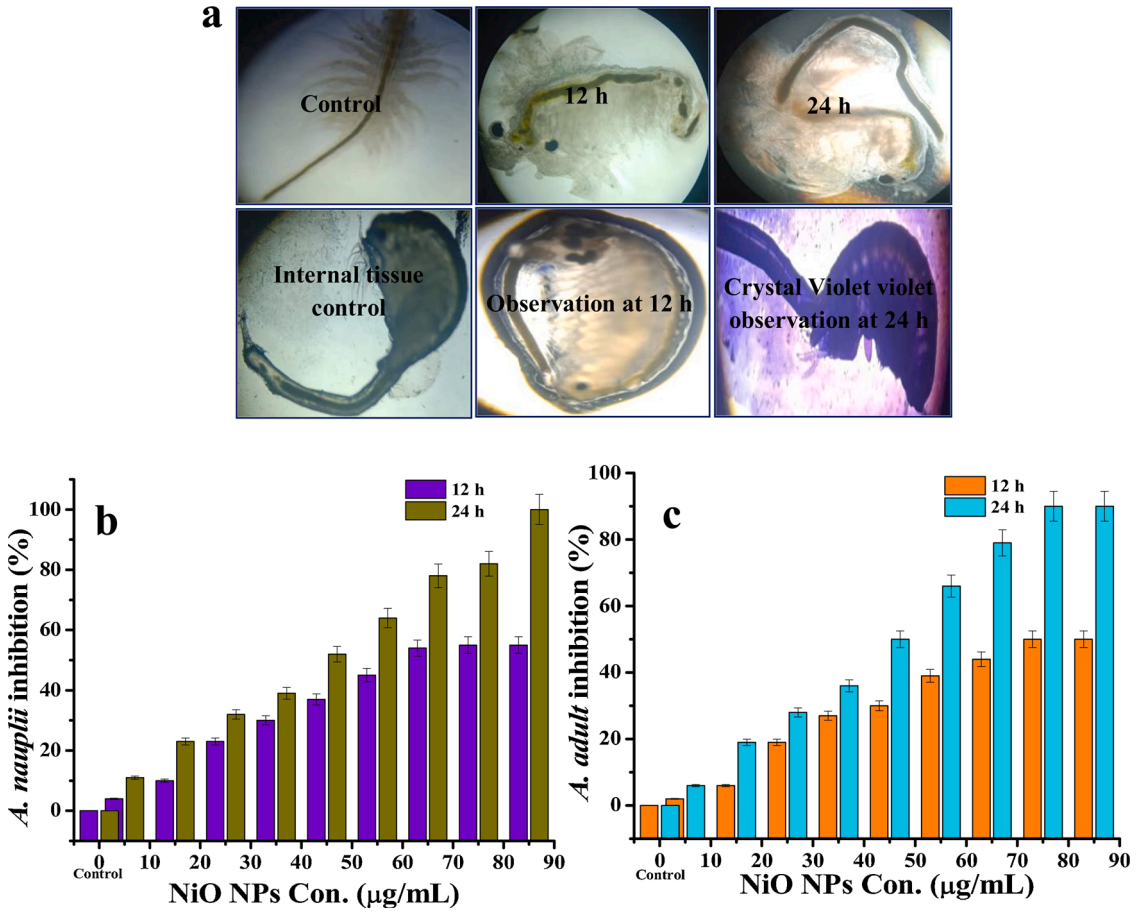

Fig. 9. Evaluation of the toxicity effect of NiO NPs against *A. franciscana* based on the mortality, internal damage (a), and differentiation of the mortality rate due to the increasing concentrations of NiO NPs at 12 h (b) and 24 h (c) time intervals.

cells of *P. aeruginosa* (Fig. 8a, b). Smooth membrane and swarming morphology of untreated control cells were observed in Fig. 8c. The bacterial attachment totally collapsed and some cellular components leakages were observed in the treated *P. aeruginosa*. The observed SEM result proved that the treated cells were affected with continuous cell death upon addition of NiO NPs. A previous study by Krishna Kumar et al. [45] found that NPs are a new weapon for inhibiting biofilm-forming cell multiplication. The NP derived material stops the exopolysaccharide production by targeting cell walls with modification or folic acid and altering metabolic pathways, including protein or DNA replication [46]. Our results are in agreement with earlier studies [11, 47] that determined that the anti-biofilm metabolites of nanoparticles are effective against biofilm-forming uropathogens in a concentration-dependent manner. Therefore, the SEM results suggest that NiO NPs enhance effectively the anti-biofilm ability against *P. aeruginosa*.

The attachment of the NiO NPs onto the surface of *P. aeruginosa* bacterial cells has shown to strongly disrupt the integrity of the bacterial membrane, thus making cells prone to cellular leakage and subsequent cell death [48]. The dispersed NiO NPs influenced bacterial growth by targeting cell walls damage or folic acid and altering metabolic pathways, including protein or DNA replication [49]. The obtained results demonstrated that NiO NPs have strong anti-biofilm activity towards selected *P. aeruginosa* bacterial strains.

3.2.11. In-vivo toxicity assessment

The toxicity assay of NiO NPs against *A. franciscana* revealed that their lethal doses or a lethal concentration for nauplii (LD50 or LC50) was 75 µg/mL at 12 h interval. The mortality rate was reported based on the concentration of NiO NPs. As a result, a minimum mortality of 15 % was observed at 10 µg/mL concentration and a maximum mortality of 50 % was observed at 75 µg/mL after 12 h. Additionally, 23 % of mortality was recorded at a concentration of 10 µg/mL and 100 % of mortality was recorded at a concentration of 80 µg/mL after 24 h. The regression values varied in nauplii and adult due to the concentration of the NiO NPs (R^2 = 0.959 and 0.955) over a 12 and 24 h period, respectively (Fig. 9b, c). Furthermore, the mortality of the NiO NPs treated *A. franciscana* was of 90 % inhibition at 75 µg/mL when compared to the untreated control. In addition, the internal damage of the NiO NPs treated *A. franciscana* adults' lungs showed damaged morphology when compared with control (Fig. 9a). The resulting microscopy images also confirmed that NiO NPs possess relatively high toxicity against *A. franciscana* nauplii.

4. Conclusion

This study introduces a novel method for synthesizing rod-shaped NiO NPs as evidenced by transmission electron microscopy. In addition, the thermal stability of the synthesized NiO NPs was studied, along with other attractive features. The excellent antibacterial, anti-QS, and anti-biofilm properties of the NiO NPs were confirmed by performing various *in vitro* experiments. The anti-biofilm mechanism of the NiO NPs was identified and found to relate to structural damage and extracellular shape modification as evidenced by using confocal laser scanning and scanning electron microscopies. Furthermore, the *in vivo* toxicity evaluation of the NiO NPs against *A. franciscana* indicated that they possess relatively high toxicity. As a result, this form of NiO NPs possesses excellent potential to fight against *P. aeruginosa* in applications where its

biofilm formation still remains a challenge.

Author statement

MM and GR designed entire manuscript. MM and GR carried out NiO NPs synthesis and biological experiments respectively. FQ and WJL provided all the facility and corrected throughout of the manuscript. MM and GR coordinated all parts of the manuscript. Finally, all the authors read and approved the final manuscript.

Declaration of Competing Interest

The authors report no conflicts of interest.

Acknowledgments

Dr. M. Maruthupandy and Dr. F. Quero acknowledge the financial support from FONDECYT (Chile) under the Postdoctoral Fellowship No. 3180128. Dr.G. Rajivagndhi and Professor Wen-Jun Li gratefully acknowledge the National Natural Science Foundation of China (Project Approval Numbers: 41950410573, 91951205 and 31670009) and Postdoctoral Science Foundation of China (Project Approval Number: 2019M663213) for financial support for this work.

References

[1] H. Heidari, M. Hadadi, H. Sedigh Ebrahim-Saraie, A. Mirzaei, A. Taji, S.R. Hosseini, et al., Characterization of virulence factors, antimicrobial resistance patterns and biofilm formation of*Pseudomonas aeruginosa* and *Staphylococcus spp*. strains isolated from corneal infection, J. Francais D' Ophtalmologie 41 (2018) 823–829.

[2] E. Noumi, M. Snoussi, A. Merghni, F. Nazzaro, G. Quindós, G. Akdamar, et al., Phytochemical composition, anti-biofilm and anti-quorum sensing potential of fruit, stem and leaves of *Salvadora persica L*. methanolic extracts, Microb. Pathog. 109 (2017) 169–176.

[3] A. Kannappan, B. Balasubramaniam, R. Ranjitha, R. Srinivasan, I.A.S. V. Packiavathy, K. Balamurugan, et al., In vitro and in vivo biofilm inhibitory efficacy of geraniol-cefotaxime combination against *Staphylococcus spp*, Food Chem. Toxicol. 125 (2019) 322–332.

[4] K.R. Devi, S. Srinivasan, A.V. Ravi, Inhibition of quorum sensing-mediated virulence in *Serratia marcescens* by *Bacillus subtilis* R-18, Microb. Pathog. 120 (2018) 166–175.

[5] S. Ilk, N. Sağlam, M. Özgen, F. Korkusuz, Chitosan nanoparticles enhances the anti-quorum sensing activity of kaempferol, Int. J. Biol. Macromol. (2017) 653–662.

[6] J.M. George, A. Antony, B. Mathew, Metal oxide nanoparticles in electrochemical sensing and biosensing: a review, Microchim. Acta 185 (2018) 358, https://doi.org/10.1007/s00604-018-2894-3.

[7] J. Jiang, J. Pi, J. Cai, The advancing of zinc oxide nanoparticles for biomedical applications, Bioinorg. Chem. Appl. (2018), 1062562.

[8] A. Hasan, M. Morshed, A. Memic, S. Hassan, T.J. Webster, H. El-Sayed Marei, Nanoparticles in tissue engineering: applications, challenges and prospects, Int. J. Nanomedicine 13 (2018) 5637–5655.

[9] B. Issa, I.M. Obaidat, B.A. Albiss, Y. Haik, Magnetic nanoparticles: surface effects and properties related to biomedicine applications, Int. J. Mol. Sci. 14 (2013) 21266–21305.

[10] A.C. Gandhi, S.Y. Wu, Strong deep-level-emission photoluminescence in NiO nanoparticles, Nanomaterials (Basel) 7 (2017) 231.

[11] L. Yu, F. Shang, X. Chen, J. Ni, L. Yu, M. Zhang, et al., The anti-biofilm effect of silver-nanoparticle-decorated quercetin nanoparticles on a multi-drug resistant Escherichia coli strain isolated from a dairy cow with mastitis, Peer J. 6 (2018) e5711.

[12] M.I. Din, A. Rani, Recent advances in the synthesis and stabilization of nickel and nickel oxide nanoparticles: a green adeptness, Int. J. Anal. Chem. (2016), 3512145.

[13] P. Pattanayak, F. Papiya, V. Kumar, N. Pramanikd, P.P. Kundu, Deposition of Ni–NiO nanoparticles on the reduced graphene oxide filled polypyrrole: evaluation as cathode catalyst in microbial fuel cells, Sustain. Energy Fuels 3 (2019) 1808–1826.

[14] G. Rajivgandhi, M. Maruthupandy, F. Quero, W.J. Li, Graphene/nickel oxide nanocomposites against isolated ESBL producing bacteria and A549 cancer cells, Mater. Sci. Eng. C 102 (2019) 829–843.

[15] V. Helan, J. Joseph Prince, N.A. Al-Dhabi, M.V. Arasub, A.G. Ayeshamariam, Madhumitha, Neem leaves mediated preparation of NiO nanoparticles and its magnetization, coercivity and antibacterial analysis, Result Phys. 6 (2016) 712–718.

[16] G. Rajivgandhi, R. Vijayan, M. Maruthupandy, B. Vaseeharan, N. Manoharan, Anti-biofilm effect of Nocardiopsis sp. GRG 1 (KT235640) compound against biofilm forming Gram negative bacteria on UTIs, Microb. Pathog. 118 (2018) 190–198.

[18] M. Maruthupandy, G. Rajivgandhi, T. Muneeswaran, J.M. Song, N. Manoharan, Biologically synthesized ZnO NPs as nanoantibiotics against ESBLs producing gram negative bacteria, Microb. Pathog. 121 (2018) 224–231.

[22] M. Alagiri, S. Ponnusamy, C. Muthamizhchelvan, Synthesis and characterization of NiO nanoparticles by sol–gel method, J. Mater. Sci. Mater. Electron. 23 (2012) 728–732.

[23] V. Kalam, A.G. Al-Sehemi, A.S. Al-Shihri, G. Du, T. Ahmad, Synthesis and characterization of NiO nanoparticles by thermal decomposition of nickel linoleate and their optical properties, Mater. Charact. 68 (2012) 77–81.

[24] S. Suresh, S. Karthikeyan, P. Saravanan, K. Jayamoorthy, Comparison of antibacterial and antifungal activities of 5-amino-2-mercaptobenzimidazole and functionalized NiO nanoparticles, Int. J. Mod. Sci. 2 (2016) 188–195.

[25] S.K. Khawlah, M.S. Ghassan, A.K. Farah, A. Abdul, N. Giuliana, Synthesis, characterization and antibacterial activity of colloidal NiO nanoparticles, J. Pharm. Sci. 29 (2016) 541–546.

[26] K. Zhang, J. Ran, B. Zhu, H. Ju, J. Yu, L. Song, et al., Nanoconfined Nickel@Carbon core-shell cocatalyst promoting highly efficient visible-light photocatalytic H2 production, Small 14 (2018) 1801705.

[27] T.Y. Yung, L.Y. Huang, T.Y. Chan, K.S. Wang, T.Y. Liu, P.T. Chen, et al., Synthesis and characterizations of Ni and NiO nanoparticles on PDDA modified graphene for oxygen reduction reaction, Nanoscale Res. Lett. 9 (2014) 444.

[28] V. Dogra, G. Kaur, A. Kaur, R. Kumar, S. Kumar, In vitro assessment of antimicrobial and genotoxic effect of metallosurfactant based nickel hydroxide nanoparticles against *Escherichia coli* and its genomic DNA, Colloids Surf. B Biointerfaces 170 (2018) 99–108.

[29] H.D. Lu, A.C. Spiegel, A. Hurley, L.J. Perez, K. Maisel, K. Ensign, et al., Modulating Vibrio cholerae quorum-sensing-controlled communication using autoinducer-loaded nanoparticles, Nano Lett. 15 (2015) 2235–2241.

[30] H. Thanh Nguyen, F.M. Goycoolea, Chitosan/cyclodextrin/TPP nanoparticles loaded with quercetin as novel bacterial quorum sensing inhibitors, Molecules 22 (2017) pii: E1975.

[31] M. Maruthupandy, G. Rajivgandhi, T. Muneeswaran, T. Vennila, F. Quero, J. M. Song, Chitosan/silver nanocomposites for colorimetric detection of glucose molecules, Int. J. Biol. Macromol. 121 (2019) 822–828.

[32] L. Akyuz, M. Kaya, M. Mujtaba, S. Ilk, I. Sargin, A.M. Salaberria, et al., Supplementing capsaicin with chitosan-based films enhanced the anti-quorum sensing, antimicrobial, antioxidant, transparency, elasticity and hydrophobicity, Int. J. Biol. Macromol. 115 (2018) 438–446.

[33] S. Hayat, S. Muzammil, B. Shabana, B. Aslam, M.H. Siddique, M. Saqalein, Quorum quenching: role of nanoparticles as signal jammers in gram-negative bacteria, Future Microbiol. 14 (2019) 61–72.

[34] B. Gómez-Gómez, L. Arregui, S. Serrano, A. Santos, T. Pérez-Coronaa, Y. Madrid, Selenium and tellurium-based nanoparticles as interfering factors in quorum sensing-regulated processes: violacein production and bacterial biofilm formation, Metallomics 11 (2019) 1104–1114.

[35] J. Rajkumari, S. Borkotoky, A. Murali, K. Suchiang, S.K. Mohanty, S. Busi, Attenuation of quorum sensing controlled virulence factors and biofilm formation in *Pseudomonas aeruginosa* by pentacyclic triterpenes, betulin and betulinic acid, Microb. Pathog. 118 (2018) 48–60.

[36] M. Alipour, Z.E. Suntres, R.M. Lafrenie, A. Omri, Attenuation of *Pseudomonas aeruginosa* virulence factors and biofilms by co-encapsulation of bismuth-ethanedithiol with tobramycin in liposomes, J. Antimicrobial Chemother. 65 (2010) 684–693.

[37] T. Li, D. Wang, N. Liu, Y. Ma, T. Ding, Y. Mei, Y, et al., Inhibition of quorum sensing controlled virulence factors and biofilm formation in *Pseudomonas fluorescens* by cinnamaldehyde, Int. J. Food Microbiol. 269 (2018) 98–106.

[38] G. Rajivgandhi, M. Maruthupandy, T. Muneeswaran, M. Anand, N. Manoharan, Anti-biofilm activity of zinc oxide nanosheets (ZnO NSs) using Nocardiopsis sp. GRG1 (KT235640) against MDR strains of gram negative Proteus mirabilis and Escherichia coli, Process. Biochem. 67 (2018) 8–18.

[39] L. Argueta-Figueroa, R.A. Morales-Luckie, R.J. Scougall-Vilchis, O.S. Olea-Mejía, Synthesis, characterization and antibacterial activity of copper, nickel and bimetallic Cu–Ni nanoparticles for potential use in dental materials, Prog. Nat. Sci. 24 (2014) 321–328.

[40] R. Soumyadipta, G. Srabanti, C. Sayantani, M. Soumya Sundar, S.P. Moulika, S. C. Bhattacharya, Controlled synthesis of spin glass nickel oxide nanoparticles and evaluation of their potential antimicrobial activity: a cost effective and eco friendly approach, RSC Adv. 19348 (2013).

[41] N. Abed, F. Saïd-Hassane, F. Zouhiri, J. Mougin, V. Nicolas, D. Desmaële, et al., An efficient system for intracellular delivery of beta-lactam antibiotics to overcome bacterial resistance, Sci. Rep. 27 (2015) 13500.

[42] M. Klinger-Strobe, J. Ernst, C. Lautenschläger, M.W. Pletz, D. Fischer, O. Makarewicz, A blue fluorescent labeling technique utilizing micro- and nanoparticles for tracking in LIVE/DEAD® stained pathogenic biofilms of *Staphylococcus aureus* and *Burkholderia cepacia*, Int. J. Nanomed. 11 (2016) 575–583.

[43] N. Cerca, F. Gomes, S. Pereira, P. Teixeira, R. Oliveira, Confocal laser scanning microscopy analysis of *S. Epidermidis* biofilms exposed to farnesol, vancomycin and rifampicin, BMC Res. Notes 16 (2012) 244.

[44] S. Saleem, B. Ahmed, M.S. Khan, M. Al-Shaeri, J. Musarrat, Inhibition of growth and biofilm formation of clinical bacterial isolates by NiO nanoparticlessynthesized from Eucalyptus globulus plants, Microb. Pathog. 111 (2017) 375–387.

[45] P. Krishna Kumar, T. Muktanand, P. Nidhi, A. Ashish Kumar, G. Shilpkala Md, A. Meraj, et al., Alginate lyase immobilized chitosan nanoparticles of ciprofloxacin for the improved antimicrobial activity against the biofilm associated mucoid P. aeruginosa infection in cystic fibrosis, Int. J. Pharm. 563 (2019) 30–42.

[46] Z. Song, Y. Wu, H. Wang, H. Han, H, Synergistic antibacterial effects of curcumin modified silver nanoparticles through ROS mediated pathways, Mater. Sci. Eng. C 99 (2019) 255–263.
[47] S.M. Navarro Gallón, E. Alpaslan, M. Wang, P. Larese-Casanova, M.E. Londoño, L. Atehortúa, Characterization and study of the antibacterial mechanisms of silver nanoparticles prepared with microalgal exopolysaccharides, Mater. Sci. Eng. C 99 (2019) 685–695.
[48] P. Budeli, R.C. Moropeng, L. Mpenyana-Monyatsi, M.N.B. Momba, Inhibition of biofilm formation on the surface of water storage containers using bios and zeolite silver-impregnated clay granular and silver impregnated porous pot filtration systems, PLoS One 13 (2018), e0194715.
[49] H.M. Hou, F. Jiang, G.L. Zhang, J.Y. Wang, Y.H. Zhu, X.Y. Liu, Inhibition of Hafnia alvei H4 biofilm formation by the food additive dihydrocoumarin, J. Food Prot. (2017) 842–847, https://doi.org/10.4315/0362-028X.JFP-16-460.